EUROPEAN ORGANIZATION FOR NUCLEAR RESEARCH
Laboratory for Particle Physics

Departmental Report **CERN/AT 2008-28**

COMPARING THERMAL STABILITY OF NbTi AND Nb_3Sn WIRES

M. Breschi[1], L. Trevisani[1],
L. Bottura[2], A. Devred[3] and F. Trillaud[4]

The investigation of quenching in low temperature superconducting wires is of great relevance for a proper design of superconductive cables and magnets. This paper reports the experimental results of a vast measurement campaign of quench induced by laser pulses on NbTi and Nb_3Sn wires in pool boiling Helium I. A comparison of the quench behavior of two typical NbTi and Nb_3Sn wires is shown from different standpoints. Different qualitative behaviors of the voltage traces recorded during quenches and recoveries on NbTi and Nb_3Sn wires are reported and analyzed. It is shown that the Nb_3Sn wire exhibits a quench or no-quench behavior, whereas quenches and recoveries are exhibited by the NbTi wire. The two wires are also compared considering the behaviors of the two main parameters describing quench, i.e. quench energies and quench velocities, with respect to operation current and pulse duration and magnetic field. It is shown that the Nb_3Sn wire exhibits a 'kink' of the quench energy vs current curve that makes the quench energy of Nb_3Sn lower than that of NbTi at some intermediate current levels. Both the qualitative differences of the voltage traces and the different behaviors of quench energies and velocities are interpreted through a coupled electromagnetic- thermal model, with special emphasis on the detailed description of heat exchange with liquid helium.

CERN-AT-2008-028
20/10/2008

1 University of Bologna, Italy.
2 CERN, Geneva, Switzerland.
3 ITER I/O, Cadarache, France.
4 LBNL, Berkeley, USA.

CERN
Accelerator Technology Department
CH - 1211 Geneva 23
Switzerland

20 October 2008

Comparing Thermal Stability of NbTi and Nb_3Sn wires

M. Breschi[1], L. Trevisani[1],
L. Bottura[2], A. Devred[3] and F. Trillaud[4]

[1]University of Bologna, Italy, [2]CERN, Geneva, Switzerland,
[3]ITER I/O, Cadarache, France, [4]LBNL, Berkeley, USA

Abstract

The investigation of quenching in low temperature superconducting wires is of great relevance for a proper design of superconductive cables and magnets. This paper reports the experimental results of a vast measurement campaign of quench induced by laser pulses on NbTi and Nb_3Sn wires in pool boiling Helium I. A comparison of the quench behavior of two typical NbTi and Nb_3Sn wires is shown from different standpoints. Different qualitative behaviors of the voltage traces recorded during quenches and recoveries on NbTi and Nb_3Sn wires are reported and analyzed. It is shown that the Nb_3Sn wire exhibits a quench or no-quench behavior, whereas quenches and recoveries are exhibited by the NbTi wire. The two wires are also compared considering the behaviors of the two main parameters describing quench, i.e. quench energies and quench velocities, with respect to operation current and pulse duration and magnetic field. It is shown that the Nb_3Sn wire exhibits a 'kink' of the quench energy vs current curve that makes the quench energy of Nb_3Sn lower than that of NbTi at some intermediate current levels. Both the qualitative differences of the voltage traces and the different behaviors of quench energies and velocities are interpreted through a coupled electromagnetic- thermal model, with special emphasis on the detailed description of heat exchange with liquid helium.

Keywords: Superconducting wires, Quench modeling, Thermal stability

1. Introduction

The recent developments of magnet technology for nuclear fusion [1] and particle accelerators [2] push towards the realization of increasingly high field magnets. Low Temperature Superconducting (LTS) wires cooled with Liquid Helium (LHe) have been widely adopted for these applications, in which they often have to work at the limits of their current carrying capabilities. In these conditions, the deposit of very small amounts of thermal energy on parts of the conductor can drive the transition from the superconducting to the normal state. These energy deposits can be caused by several events, such as conductor motion, stick-slip friction, cracks of the epoxy resin used for impregnation, particle showers in accelerators and absorption of energetic particles in magnets for thermonuclear fusion experiments [1]. In some cases, an efficient heat removal through conduction along the wires and heat transfer towards liquid helium can restore the superconducting state existing before the energetic disturbance (recovery). In other cases, the 'normal zone' can expand along the conductor (quench), often requiring a fast de-energization of the magnet to avoid permanent damages [3].

The experimental and numerical analyses of quench are of paramount importance for a proper design of superconducting devices, and have been carried out extensively since the 1970's both on wires and magnets [3, 4, 5]. A correct evaluation of the minimum energy that determines an irreversible transition (Quench Energy, QE) and of the velocity of propagation of the normal zone (Normal Zone Propagation Velocity, NZPV) can allow the design and protection of magnets safely operating at their highest level of current density.

This paper reports the analysis of an extensive experimental activity on quench development and propagation in LTS wires in pool boiling LHe carried out at CEA Saclay [6, 7]. Quench was induced in NbTi and Nb_3Sn wires through illumination with a pulse diode laser. The QEs and NZPVs were measured at different transport currents, magnetic fields, and pulse time durations. The experimental data revealed remarkable qualitative and quantitative differences between NbTi and Nb_3Sn wires quench behaviors. In this paper a detailed numerical model of quench development and propagation in LTS wires is described, which allows a deeper insight in the physical phenomena occurring in these wires and the interpretation of their different behaviors.

The modeling of quench in superconducting wires requires a coupled electrical-thermal model of the wire itself. Several analytical or numerical analyses of quench in single wires reported in the literature [3, 4, 9] are based on the assumption that the temperature and voltage are uniform over the wire cross section, thus describing quench with a 1-D model. The present analysis shows that this assumption can be inadequate to describe precisely quench propagation in some cases of relevance. Especially for Nb_3Sn wires, it is necessary to account for a finite transverse electrical and thermal resistances of the

wire matrix to achieve a description of the quench phenomena in good agreement with experimental data.

One of the crucial aspects of these analyses is the description of heat exchange with pool boiling LHe. Experimental and theoretical activities have been carried out to describe the different phases of heat exchange between a solid surface and LHe [10, 11], which involve several physical phenomena, such as the Kapitza temperature discontinuity, the transition from nucleate to film boiling, and the characteristic thermal 'hysteresis' occurring in the inverse transition from film to nucleate boiling [11]. The model presented here takes into account these phenomena, emphasizing the role of a detailed description of heat exchange with liquid helium for the correct interpretation of the experimental results. A special consideration is given to the simulation of the spatial and temporal build up of the film boiling phase. Following [11], an energetic criterion is adopted to compute the time of onset of film boiling, while a spatial smearing factor is introduced here to account for a smoothed transition along the wire length.

2. Experimental setup

The measurements were performed on NbTi and Nb_3Sn wires of 0.8 mm diameter, with an active sample length of 8 cm, refrigerated in pool boiling LHe at 4.2 K [6]. The wire was illuminated with a single-mode diode laser over a 0.8 mm region centered in its middle section, with variable energy inputs and pulse durations (in the range from 15 μs to 2 ms). The experiments were carried out at different transport currents and background magnetic flux densities. For each set of parameters, the wire critical current was measured in situ before inducing quenches through external energy input. The experiments were repeated with different energy inputs in order to determine the QE in each condition. The voltages developed along the sample were measured through a set of voltage taps illustrated in Fig. 1. The voltage taps to measure voltage V_1 were positioned across the illuminated region of the wire, whereas the voltage taps to measure V_2 and V_3 were attached along the wire at some distance from the illuminated zone. The relative distances of voltage taps for the three measurements V_1, V_2 and V_3 are 5.9 mm, 7.2 mm and 7.3 mm respectively for the NbTi wire and 7.4 mm, 7.0 mm and 7.2 mm respectively for the Nb3Sn wire. The NZPV was evaluated from the time-of-flight of the voltage increase measured at the location of the voltage taps V_2 and V_3.

The cross section of the NbTi wire adopted in the experiments is shown in Fig. 2a. The wire is an LHC-type (02), Cu/NbTi wire with 0.825-mm diameter and a Cu/NbTi ratio equal to 1.95. The superconducting filaments (with a diameter of 6 μm) are embedded in the outer Cu matrix.

The cross section of the un-reacted Nb_3Sn wire realized with Internal Tin technology is shown in Fig. 2b. The wire has the same diameter of 0.825 mm as the NbTi wire and

consists of five different metal phases. The wire is subdivided into 19 multi-filamentary sub-elements with a diameter of about 110 μm, each including 198 Nb-7.5wt.%/Ta filaments with a diameter of 4 μm. The multi-filamentary area is surrounded by a mixed Nb/Ta diffusion barrier, and an outer Cu stabilizing matrix. After heat treatment, the copper included inside the anti-diffusion barrier turns into a Cu/Sn matrix. The thermal and electrical conductivity of this material at 4.2 K can be some orders of magnitude lower than that of pure copper.

3. Numerical Model

3.1. *Thermo-electrical model of the superconducting wires*

A coupled thermo-electromagnetic model of the superconducting wire is obtained by subdividing the wire into *Ns* sectors along the length and *Ne* elements in the wire cross section. From the electrical point of view, each element is described as the parallel between a superconducting and a normal conducting part. The *E-J* characteristics of the superconductor is defined by the widely adopted 'power law' [3], with temperature and field dependant critical current as in [14] for NbTi and as in [15] for Nb_3Sn. Since the characterization of the NbTi and Nb3Sn wires used in the experiments was only available at 4.2 K, a number of critical surface parameters were set to typical values reported in literature [14, 15]. The different electrical elements in each sector are connected through transverse electrical resistances. The general non linear electrical lumped parameters circuit is represented in Fig. 3.

The thermal model computes the temperatures of each element *j* in sector *i* on the basis of the following set of equations:

$$m_{i,j} c_{pi}\left(T_{i,j}\right)\frac{dT_{i,j}}{dt} = p_{J,i,j} + p_{cond,i,j} + \sum_{k}\frac{T_{i,j} - T_{i,k}}{R_{\mathrm{TH},i,j,k}} + p_{ext,i,j} - p_{He,i,j} \qquad (1)$$

where m, c_p, and T are the mass, specific heat at constant pressure and temperature. The Joule power p_J couples the thermal model to the electrical model and accounts for the dissipation due to both longitudinal and transverse currents. The term p_{cond} accounts for the thermal conduction along the strand axis, while transverse heat flux between adjacent elements are evaluated using a lumped thermal resistances R_{TH}. The term p_{He} represents the thermal power towards the liquid helium bath for the external elements, and is computed through the model of heat exchange with pool boiling helium I, described in the next section. The term p_{ext} represents the thermal power from the Diode Laser and differs from zero only for the illuminated elements in the middle of the wire.

The temperature dependent properties of copper, NbTi and Nb_3Sn are based on the Cryosoft database [16]. For the Nb_3Sn wire, the electrical and thermal properties of the Cu-Sn alloy were derived from [17].

3.2 *Heat exchange with pool boiling LHe.*

The phenomenon of heat exchange with boiling liquid helium takes place in different regimes depending on the temperature gradient and heat flux. At low heat flux vapor bubbles form at different nucleation sites on the heated surface. Initially, the bubbles are separated from each other allowing a good thermal contact of the bulk fluid with the surface. This regime is referred to as nucleate boiling. As the heat flux increases, the bubbles start coealescing until a thin evaporated film of helium gas is formed close to the heated surface. This regime, where the heat exchange coefficient abruptly drops due to the low conductivity of the vapor film, is referred to as film boiling. Several experiments have been carried out to assess the transient nucleate-boiling heat-transfer coefficients [10, 11, 13]. The measured data are strongly dependent on several parameters, such as the surface material, roughness, and condition (clean, oxidized, coated, etc.). In the conditions considered here, i.e. in the range of cryogenic temperature associated with the use of liquid helium, the Kapitza resistance [12] cannot be neglected. In the model adopted here, it is assumed that in the first phase of heat exchange (up to tens of μs in the present case, in which relevant convective motions cannot be established) the Kapitza effect represents the main limiting thermal resistance. The nucleate boiling heat exchange coefficient is estimated as

$$h_{nucl,i,j} = \frac{Q_{Kap}}{S_i^{wet}\left(T_i - T_{He}\right)} = \frac{A\left(T_s^m - T_{He}^m\right)}{S_i^{wet}\left(T_i - T_{He}\right)} \qquad (2)$$

where Q_{kap} is the Kapitza thermal flux, T_s and T_{He} are the wire surface and helium bath temperatures and A is a constant coefficient. The parameters A = 242 W/m^{2}K^m and m = 2.8 in (2) have been determined by fitting the experimental data. The values found are in the range of those indicated in [13]. With a given thermal flux towards helium, the formation of a continuous vapor film around the wire surface requires a certain time. Several experimental investigations have been published that correlate the time of onset of film boiling (t_{on}) with the total energy transferred to the helium up to the film boiling formation, for a constant power flux towards helium [3, 11]. In this work, following the approach of [11], the experimental correlation between onset time and deposited energy is extended to the general case of variable flux power towards helium through the following formula:

$$E_{\lim} = \alpha\, t_{on}^{\,n} \qquad (3)$$

where α is a constant coefficient. In our computations, we use: α = 720 J/m^{2}s^n and n = 0.6, in the range of the values reported in the literature [13]. After E_{lim} is reached, the heat transfer coefficient drops to its film boiling value, h_{film}, taken equal to 250 W/m^{2}K, a value compatible with most measurements performed on copper wires.

A final element in the heat transfer model is the observation that in steady-state experiments film boiling is never reached, even after a long time, if the heat flux remains below a threshold value, q. In these cases, the nucleate boiling can in fact remove the heat transferred to the helium without forming a vapor film [11]. These heat flux values correspond to maximum ΔT values in the range from 0.6 to 0.8 K. In the algorithm implemented in this work, the energy transferred to liquid helium is computed from each sector through numerical integration of the exchanged power. To account for the aforementioned threshold ΔT, this integration only starts after the sector ΔT temperature overcomes 0.7 K. As the integrated energy flux reaches the limit defined in (3), the sector would enter the film-boiling regime. The length of sectors required to achieve numerical convergence can be in the order of tenths of mm. A formation of stable film boiling over such a short length is however physically not possible. Indeed, the gas film formation is a collective phenomenon rather than a local transition. This problem is solved in the present approach avoiding an abrupt change of the local heat transfer coefficient between adjacent sectors. This is obtained through the introduction of a Gaussian smearing of the heat transfer coefficient along the sample length. This procedure is applied by defining for every sector the discrete functions: $H_{check}(i) = 0$ for nucleate boiling and $H_{check}(i) = 1$ when the limit defined in (3) is reached, with $i = 1, N_s$. The smeared value of the heat transfer coefficient is then given by

$$H_{smeared}(i) = \frac{\sum_{j=1}^{N_s} w(i,j) H_{check}(j)}{\sum_{j=1}^{N_s} w(i,j)} \tag{4}$$

where the weight functions w (i, j) are defined as

$$w(i,j) = \frac{1}{\sqrt{2\pi}\,\sigma} \int_{x_l(j)}^{x_r(j)} \exp\left\{ -\frac{[x_m(i) - x]^2}{2\sigma^2} \right\} dx \tag{5}$$

where x_l (j), x_r (j), and x_m (i) represent the left and right edges of element j and the central point of element i. Finally, for each sector, the heat transfer coefficient is computed as

$$h_i = [1 - H_{smeared}(i)]\, h_{nucl} + H_{smeared}(i)\, h_{film} \tag{6}$$

with $i = 1, N_s$.

This definition shows that the value of h for each sector is affected by the values of h in the neighboring sectors, allowing for a smooth transition from nucleate to film boiling.

The shape of the smearing region is controlled by the parameter σ. The effect of the introduction of this parameter is shown in Figs. 4 and 5, respectively referring to simulations performed with $\sigma = 0$ and $\sigma = 1$ mm at two different times from the beginning of the heat pulse. It can be noticed that without smearing factor, very small regions of film boiling can be attained in computations as the illuminated central sector reaches the energy limit (see Fig. 4a). This numerical result does not respect the physics of the phenomenon, as this region can be smaller than the typical diameter of one single helium bubble. Even with a larger film boiling region, the discontinuity obtained with $\sigma = 0$ in the heat exchange coefficient at the edges of the normal region defined by the temperature profile seems not physically realistic (see Fig. 4b). The effect of smoothing is illustrated in Fig. 5a and 5b that correspond to the same cases reported in Fig. 4a and 4b with σ equal to 1 mm. This value of σ is compatible with the dimension of a few adjacent helium bubbles as determined by photographic studies, that show bubble diameters in the range from 0.2 to 0.5 mm, with a peak at 0.35 mm [18, 19, 20].
To account for the hysteretic behavior of the transition from nucleate to film boiling, the heat exchange model allows wire sectors to enter the film boiling regime, and, subsequently, to recover the nucleate boiling regime if the temperature decreases. In our parameterization, this backward transition occurs at a ΔT value that in general differs from the ΔT corresponding to the transition to film boiling (hysteresis). A recovery ΔT of 0.1 K, compatible with experimental results [18], has been selected for computation. This feature of the model is essential to accurately describe the recoveries at long times, when maintaining the film boiling regime leads to an artificially low value of heat transfer coefficient.

4. Voltage traces

4.1 *Voltage traces recorded on the NbTi wire*

Experimental data for the LHC Cu/NbTi wire sample were obtained with a background field in the range from 5 to 7 T and transport currents in the range from 80% to 95% of the wire critical current. The values of the critical currents measured in situ are equal to 534 A at 5 T, 424 A at 6 T and 313 A at 7 T.
The model described in section 3 was implemented in order to reproduce the experimental voltage traces, with very satisfactory results. However, it was found in a parametric study that results in agreement with experimental data could be obtained also considering zero transverse thermal and electrical resistances. This is due to the high *RRR* of the copper matrix (set to 95 for these calculations) which directly surrounds the NbTi filaments, and provides a good thermal and electrical short circuit. The thermal model could therefore be simplified by considering only one temperature value over the wire section as follows:

$$m_i c_p(T_i)\frac{dT_i}{dt} = p_{J,i} + p_{ext,i} + p_{cond,i} - p_{He,i} \qquad (7)$$

where c_p and k are respectively the weighted averaged values of specific heat and thermal conductivity of the copper matrix and the NbTi filaments. Moreover, the solution of the

electrical circuit in Fig. 3 could be simplified by removing transverse resistors R_{EL}. These simplifications led to faster code execution, still providing results in good agreement with the experimental data.
The calculated voltage traces are compared in Fig. 6 with the experimental ones for I_{op} = 85% I_C, 6 T background field and three different light pulse durations: 50, 100 and 2000 μs. The voltage traces relative to the voltage taps located across the illuminated region (V_1) are reported for both quench and recovery. The curves relative to V_2 and V_3 only refer to the quench case. The trace relative to the laser pulse refers to the voltage across the diode laser, and is reported in arbitrary units to show the period of illumination of the wire.
The computed and experimental voltage traces show a very good agreement over the whole range of pulse lengths. The model can also reproduce the propagation of quench along the wire, as seen from the V_2 and V_3 curves. Similar agreements have been found over a wide range of transport currents and background fields.
As a general remark, it is worth noting that in most of the recovery cases analyzed, the numerical model did not show any transition to film boiling. In a few cases, with low power inputs and long pulse durations (2 ms), a local transition to film boiling over a very small region was observed, not able to drive the quench. It was found that the actual development of film boiling over a significant wire length is the key factor that prevents the wire recovery after the end of the heat income due to laser illumination. An accurate modeling of the heat exchange process with liquid helium during the transition from nucleate to film boiling is therefore of paramount importance for a correct reproduction of the experimental data.
Figure 7 shows the time evolution of the heat fluxes from the laser and towards the helium for the middle wire sector in the quench case reported in Fig. 6b. When the total energy transferred to helium at the central sector reaches the energy limit defined in (3), the heat flux transferred to the helium starts decreasing in successive small steps. These steps correspond to the onset of film boiling in neighboring sectors and result from the smearing factor described in Section 3.2, which avoids the abrupt variation of heat exchange coefficient that would be obtained with $\sigma = 0$.
The introduction of the smearing factor σ in the LHe model was the key improvement to correctly reproduce experimental data. A small value of σ leads to an abrupt drop in the heat exchange coefficient and consequently to a too fast quench development (Fig. 8). On the other hand, a value of $\sigma \approx 1$ mm leads to results in a very good agreement with the experimental data (see Fig 6a for the same case). Values of σ higher than 1 mm led to a worse agreement with experimental data, but with less influence on the simulation results than lower values.

4.2 *Voltage traces recorded on the Nb_3Sn wire*

Experimental data for the Cu/Nb_3Sn wire sample were obtained with a 7 T background magnetic field and transport currents in the range from 80% to 95% of the wire critical current, equal to 431 A. The voltage traces recorded on the Nb_3Sn strand show a different qualitative behavior of the quench development with respect to NbTi.

A first difference is the fact that in the case of Nb_3Sn wires, it is not possible to measure any significant voltage trace in the absence of quench. When the sample is subjected to a heat pulse with an energy lower than the quench energy, the voltage practically remains equal to zero. This result significantly differs from the results obtained with NbTi wires under the same conditions. As shown in Fig. 6, the recovery voltage traces recorded on NbTi strands with pulse energies slightly smaller than the QE, are clearly measurable and closely follow the voltage traces of quenches up to a 'quench decision time' at which the bifurcation occurs.

A second important difference between the voltage traces recorded with the two wires is the remarkable delay between the beginning of the laser pulse illumination and the rising of the voltage measured across the heated region in the Nb_3Sn wire during quenches. The rising of the voltage actually occurs almost at the end of the illumination period.

The simplified model that was successfully applied to the NbTi wire assuming an uniform temperature in the wire cross section and neglecting the transverse electrical resistance between the superconducting filaments and the copper matrix could not reproduce the peculiar behaviors of Nb_3Sn. As shown in Fig. 9, the calculation results of the simplified uniform temperature model applied to the Nb_3Sn wires are in blatant disagreement with the experimental voltage traces. This is also witnessed by the computed value of QE, which is about four times higher than the experimental value.

The agreement between computation and experiment could be remarkably improved by subdividing the cross section of the Nb_3Sn wire into two sub-elements and introducing appropriate values of transverse thermal and electrical resistances. In particular, in order to keep low computation times, only two sub-elements were considered at different temperatures T_1 and T_2, corresponding to the outer copper stabilizing matrix and the inner filaments/bronze area. This improvement in the modeling was sufficient to obtain results in good agreement with the experiments.

Figure 10 reports the voltage traces computed with the two-temperature model (broken lines) in comparison with the experimental ones (continuous lines) for I_{op} = 85% I_C, 7 T background field and three different light pulse durations: 50, 100 and 2000 μs. As in previous figures, the trace relative to the laser pulse refers to the voltage across the diode laser, and is reported in arbitrary units to show the period of illumination of the wire. The voltage traces computed with the two-temperature model show a rather good agreement with experimental ones over the whole range of pulse lengths.

As illustrated in Fig. 11, the two-temperature model computes extremely low voltage traces in case of pulse energies slightly lower than the QE, in accordance with experiments. Moreover, the model correctly describes the delay between the beginning of the laser illumination and the rising of the voltage traces. Figure 12 shows the evolution of the temperatures T_1 (stabilizing copper) and T_2 (inner Nb_3Sn filamentary area) of the central illuminated sector for the quench simulation reported in Fig. 10(b). The temperature of the superconducting filaments reaches the current sharing temperature of Nb_3Sn at the end of the heat pulse, with a delay from the laser pulse initiation.

On the basis of these observations, a physical interpretation of the phenomena occurring in the Nb_3Sn wire can be given. The low conductivity of the bronze matrix compared to pure copper prevents the good thermal end electrical contact of the superconducting Nb_3Sn with the stabilizing Cu matrix. This affects the stabilization effect of the outer matrix, that cannot effectively remove heat from the inner filaments when a quench

occurs. The QE provided by the diode laser therefore practically corresponds to the energy needed to heat the illuminated wire sector up to the onset of the superconducting to normal transition. Once the superconducting filaments reach their current sharing temperature, joule losses develop in the superconductor, but this heat cannot easily be removed by the copper stabilizer due to the thermal resistance mentioned above. This phenomenon explains the abrupt transition from the 'no quench' behavior without recordable voltage signals to the full quench development with the deposition of a slightly higher energy. The same phenomenon explains why the voltage across the heated region rises after a given delay from the pulse initiation, just when the total amount of energy needed to reach the current sharing temperature has been deposited. On the contrary, the embedding of NbTi filaments into the copper matrix improves the heat exchange and explains the different stability behavior of the two wires.

5. Quench Energy

5.1 *Computed and measured quench energies on the NbTi wire*

The Quench Energies (QE) calculated at 6 T and 85% of critical current for different light pulse durations are reported in Fig. 13. The same plot reports the total energy emitted by the optical fiber illuminating the wire. As expected, QEs increase with increasing pulse duration due to the partial heat removal through conduction and heat transfer to LHe during the illumination period itself. The computed QEs for long pulses are in the order of 55 to 60% of the total energy emitted by the laser. This result can be considered as a reasonable estimation of the amount of energy actually absorbed by the wire. The calculated QEs tend towards the total emitted energy for short pulses, which may be too high. This discrepancy could be due to the energetic criterion chosen for the transition from nucleate to film boiling (see Eq. (3)). This experimental criterion was in fact established for pulses in the 100-to-1000-μs range [11]. Another possible mechanism that could lead to the absorption of different fractions of the emitted energy depending on the pulse light duration is the formation of bubbles before the end of the illuminating period for long pulses. This could cause diffusion of the incoming light due to the different refractive index of cold gaseous helium with respect to liquid helium. Further investigations are needed to better understand and describe this phenomenon.

5.2 *Computed and measured quench energies on the Nb_3Sn wire*

The Quench Energies (QE) computed for the Nb_3Sn wire at 7 T and 85% of critical current for different values of light pulse durations are reported in Fig. 14. In the same plot, we also report the value of the total energy emitted by the laser. The computed QE's are in the order of 45% to 70% of the total energy emitted by the laser. Also for Nb_3Sn the quotes of absorbed energy in short and long pulses differ, but these variations are less relevant than for NbTi.

5.3 *Comparing quench energies of the NbTi and Nb_3Sn wire*

The validated model was used for the evaluation of NbTi and Nb_3Sn wires thermal stability at different values of background field and engineering current density. The comparison of results (see Fig. 15) shows that at 4.2 K the Nb_3Sn wire always performs better than the NbTi wire for background fields higher than 7 T. For lower fields, the Nb_3Sn presents higher QEs only for high or low current densities, but there is a region at intermediate current values where the NbTi wire shows better stability. It was found that the Nb_3Sn performance drop at these intermediate current densities is due to the transverse thermal and electrical conductances. Considering infinitely high transverse conductivities (uniform temperature on the cross section and perfect electrical parallel between Nb_3Sn filaments and stabilizing Cu) made the QE "kink" disappear, with Nb_3Sn always showing better performances than NbTi.

6. Quench Velocities

The last relevant parameter in the quench analysis is the velocity of quench propagation. As shown in Fig. 6 and 10, the propagation of the voltage front across voltage taps V_1 V_2 and V_3 as calculated by the model is in good agreement with experimental data, so that the estimated quench velocities are comparable. Therefore, Figure 16 only reports the measured quench velocities at different engineering current densities. From the data reported for the NbTi wire, it can be noticed that the quench velocity increases with current density and background field (by extrapolation of the plotted data) as observed in previous experiments [21] and predicted by the analytical formula for adiabatic quench propagation [3]:

$$v_{ad} = \frac{J}{\gamma c_p}\sqrt{\frac{L_0 T_s}{T_s - T_b}} \qquad (8)$$

where J is the engineering current density, γ the density, L_0 the Lorentz number, T_s the average between current sharing and critical temperature and T_b the helium bath temperature. The Nb_3Sn wire at 7 T shows lower NZPV than NbTi at 7 T extrapolated at the same current densities. This could be due to the fact that $T_s/(T_s - T_b)$ decreases with increasing T_s (which is higher in Nb_3Sn with respect to NbTi at 7 T), while the variation of the specific heat in (8) should not be very significant in this case.

Conclusions

A wide database of quench experiments on NbTi and Nb3Sn wire in pool boiling He I has been collected. An accurate modeling of these experiments has shown the relevance of a detailed description of the heat exchange with liquid helium to achieve a correct reproduction of the experimental results. An effective description of the transition from nucleate to film boiling has been obtained through the combination of an energetic criterion and two heat flux criteria. The energetic criterion computes the total amount of energy required to transit from the nucleate boiling regime to the film boiling regime. The heat flux criterion defines two main threshold values of the temperature difference between the wire surface and the helium bath. A first threshold value defines the temperature difference below which the transition does not occur even after a long time of heat deposition into the helium, in agreement with stationary heat flux experiments. The application of the energetic criterion alone cannot account for this experimental result, as the energy limit would in any case be reached after a certain time. A second threshold temperature difference defines the reverse transition from film to nucleate boiling that can occur in the case of recovery. This reverse transition occurs at a ΔT that differs from the one corresponding to the transition from nucleate to film boiling, accounting for the hysteretic behavior found in experiments. Another relevant feature of the model is the smearing of the heat exchange coefficient along the wire length, that describes this transition as a collective phenomenon rather than as a local discontinuity.

A comparison of the quench behaviors between two typical commercial wires of NbTi and Internal Tin Nb_3Sn has been carried out, considering the mechanism of development and propagation of the normal zone, and the two main parameters describing quench (Quench Energies and Normal Zone Propagation Velocities). The thermal and electrical transverse resistances of the wire matrices, made of copper for NbTi and partly made of low alloy bronze for the Nb_3Sn wire, play a relevant role in determining the qualitative differences between these two wires. The thermal resistance hinders the heat removal from the inner multifilamentary area, and leads to an abrupt transition from recovery to quench in the Nb_3Sn wire, not exhibited by the NbTi wire. This mechanism reduces the QEs of the Nb_3Sn wire used for these experiments, that in certain conditions can become lower than that of the NbTi wire. The comparison of quench velocities reveals a faster normal zone propagation in the NbTi wire than in the Nb_3Sn wire, a feature that can ease the magnet protection.

References

[1] J. H. Schultz et al.,"The ITER Central Solenoid" , 2005, Proc. Twenty-First IEEE/NPS Symposium on Fusion Engineering, pp.1 – 4, 2005.

[2] A. Devred et al., "Status of the Next European Dipole (NED) activity of the Collaborated Accelerator Research in Europe (CARE) project", *IEEE Trans. Appl. Supercond.*, Vol. 15, no. 2, pp. 1106–1112, 2005.

[3] M. Wilson, Superconducting Magnets, Clarendon Press, Oxford, 1983.

[4] L. Dresner, Stability of Superconductors, Plenum Press, New York, 1995.

[5] L. Bottura, 'Practical Stability Design', Handbook of Applied Superconductiviy, B3.3, B. Seeber, Institute of Physics Publishing, Geneva, 1998.

[6] F. Trillaud et al., "A novel technique for minimum quench energy measurements in superconductors using a single mode diode laser," *Cryogenics*, 45 (8), pp. 585–588, 2005.

[7] F. Trillaud et al., "Investigation of the stability of Cu/NbTi multifilament composite wires", *IEEE Trans. Appl. Supercond.*, 16 (2), pp. 1712–1716, 2006.

[8] M. Breschi et al., "Minimum Quench Energy and Early Quench Development in NbTi Superconducting Strands", *IEEE Trans. Appl. Supercond.*., 17 (2), pp. 2702-2705, 2007.

[9] P. Bauer, R. Wolf, L. Oberli, M. N. Wilson, "Minimum quench energies of LHC strands", *IEEE Trans. Appl. Supercond.*., 9 (1), pp. 1137-1140, 1999.

[10] W. G. Steward., "Transient helium heat transfer: phase I- static coolant", *International Journal of Heat and Mass Transfer*, Vol. 21, 1978.

[11] C. Schmidt, "Review of steady state and transient heat transfer in pool boiling He–I", Proceedings of the Saclay Workshop on Stability of Superconductors in He-I and He-II, International Institute of Refrigeration, Paris, pp. 17-31,1982.

[12] N. S. Snyder, "Heat transport through helium II: Kapitza conductance", *Cryogenics*, 10 (2), pp. 89-95, 1970.

[13] J. G. Weisend, II, Handbook of Cryogenic Engineering, Philadelphia, PA, Taylor and Francis, 1998.

[14] L. Bottura, "A practical fit for the critical surface of NbTi", *IEEE Trans. Appl. Supercond.*., 10 (1), pp. 1054-1057, 2000.

[15] D.M.J. Taylor, D.P. Hampshire, "The scaling law for the strain dependence of the electrical current density in Nb3Sn superconducting wires", *Superconductor Science and Technology*, 18, pp. S241-S252, 2005.

[16] Thea Software, Cryosoft, France, 2003.

[17] N. J. Simon, E. S. Drexler, R. P. Reed, "Properties of Copper and Copper alloys at Cryogenic Tempreatures", NIST Monograph 177, NIST, Boulder, CO, USA, 1992.

[18] B. Baudouy, CEA Saclay, Private Communication, 2007.

[19] L. Augyrond, Contribution à l'étude des écoulement duphasiques d'hélium, PhD Thesis (in French), Université Pierre et Marie Curie 6, Paris, April ,1996.

[20] H.K. Zust and W.B. Bald 'Experimental observations of flow boiling of liquid helium I in vertical channels', *Cryogenics*, 21(11), pp. 657-666, 1981.

[21] J. Miller, J. Lue, L. Dresner, 'Investigation of stability of composite superconductors in typical coil configurations', *IEEE Trans Magnetics*, 13(1), pp. 24-27, 1977.

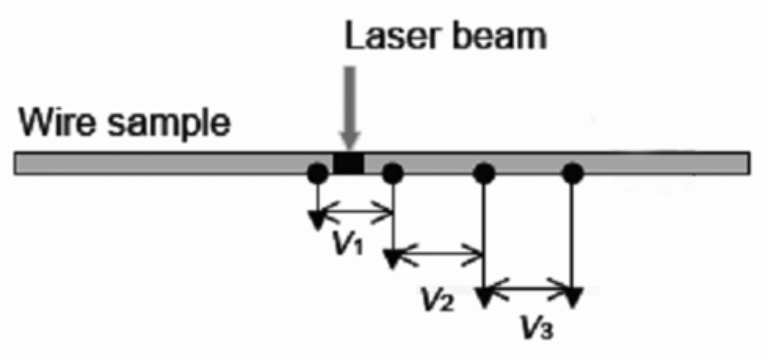

Figure 1. Schematics of the voltage taps location.

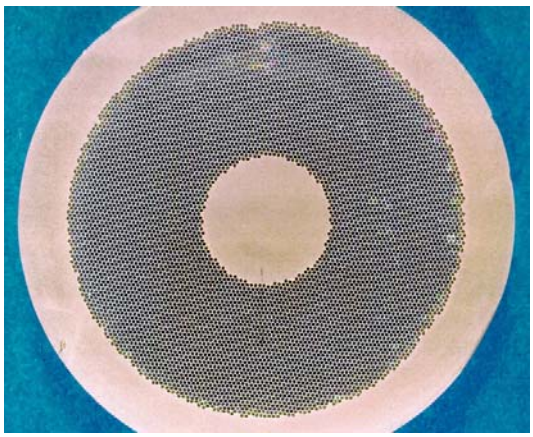

Figure 2a.

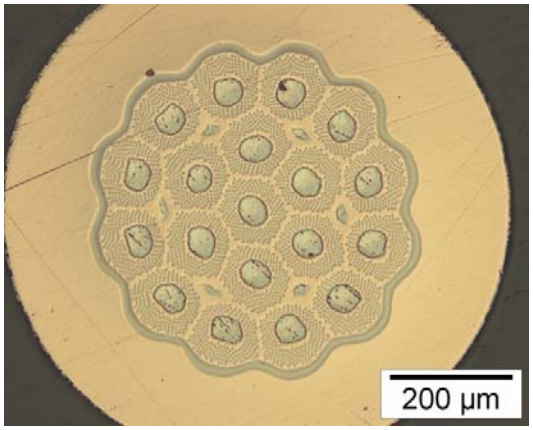

Figure 2b.

Metallographic cross section of the NbTi wire (a) and of the un-reacted Nb_3Sn wire (b) adopted in the experiments.

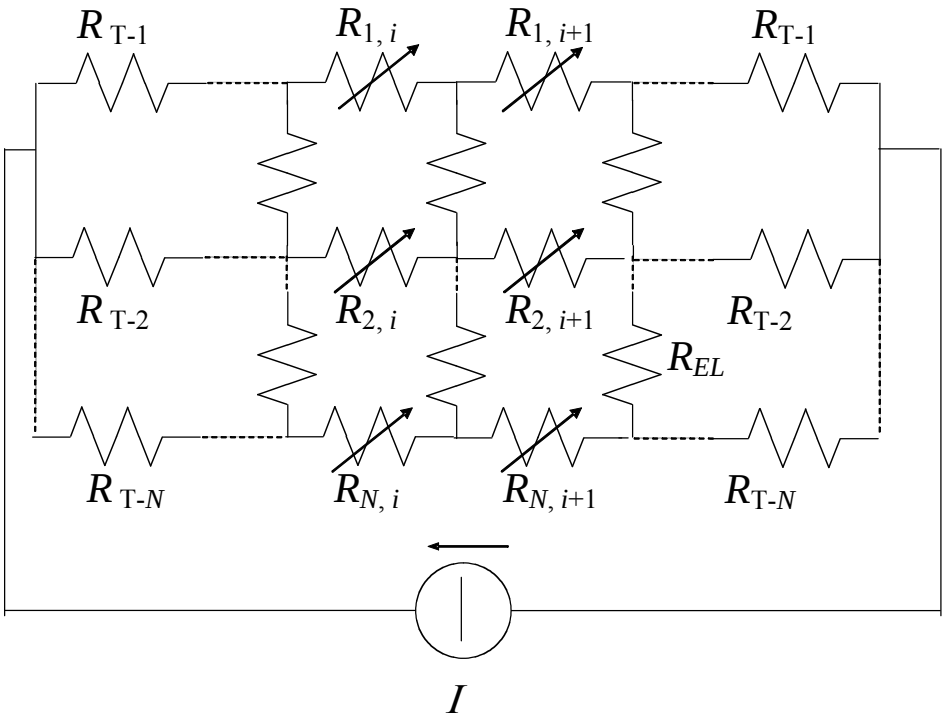

Figure 3. Schematics of the non linear electrical circuit adopted for the simulations. Each non linear resistor in the circuit in general represents the parallel of a normal and a superconducting part.

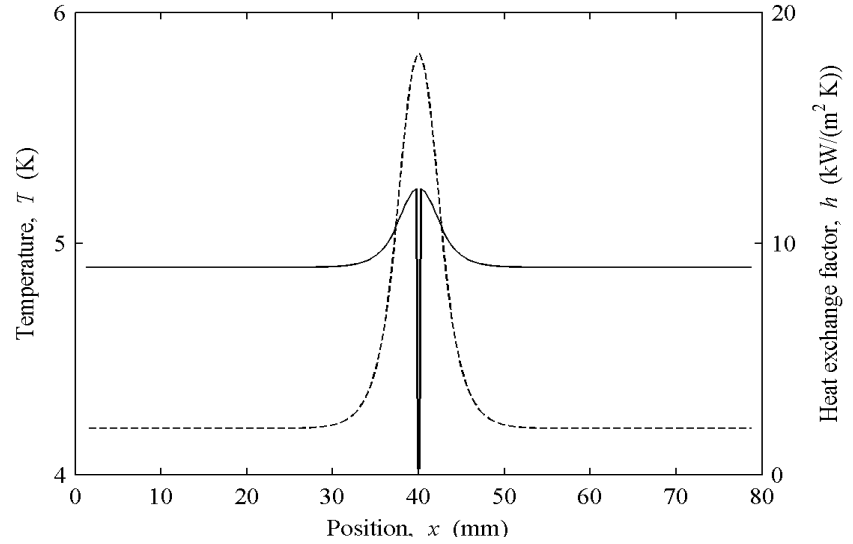

Figure 4(a).

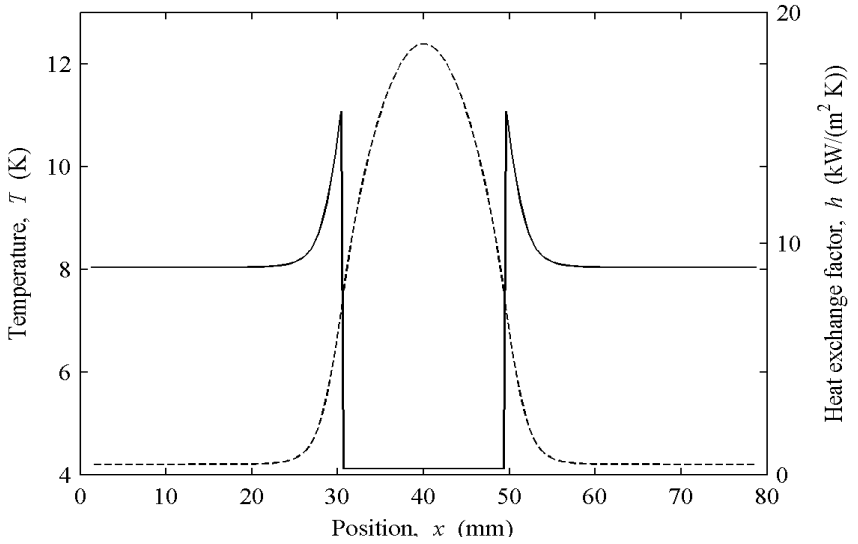

Figure 4(b).

Temperature and heat exchange coefficient profiles computed with σ = 0 mm at the beginning of the resistive transition (t = 200 μs, (a)) and after full development of a film boiling region (t = 800 μs, (b)).

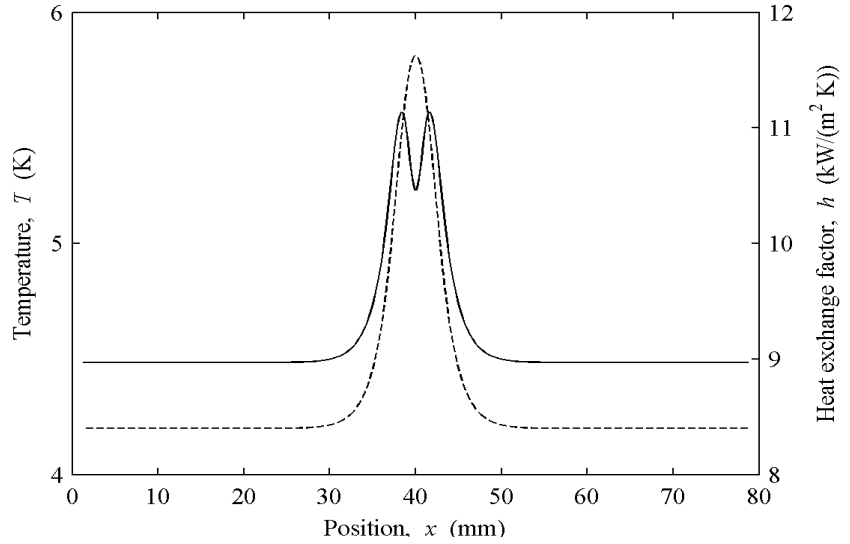

Figure 5(a).

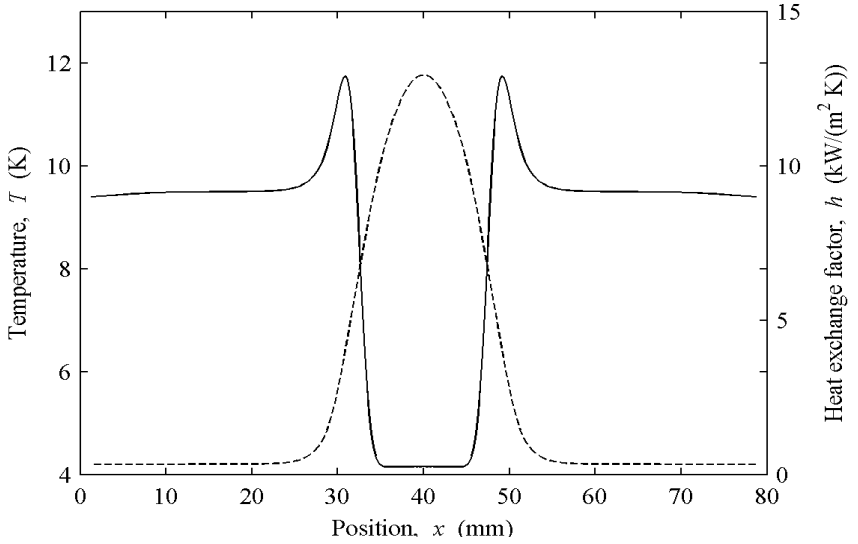

Figure 5(b).

Temperature and heat exchange coefficient profiles computed with σ = 1 mm at the beginning of the resistive transition (t = 200 μs, (a)) and after full development of a film boiling region (t = 800 μs, (b)).

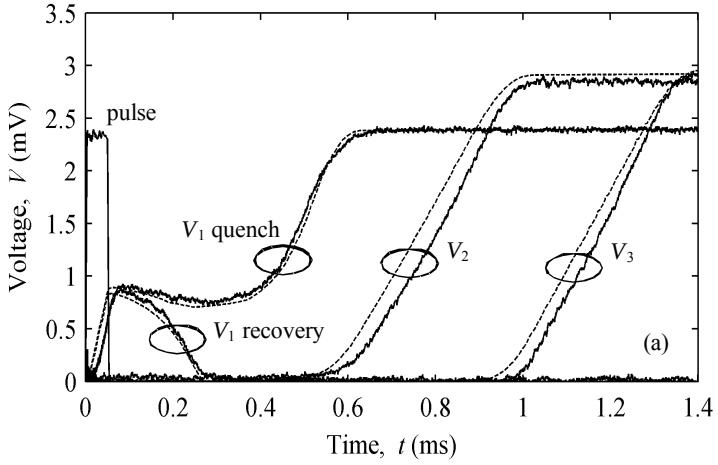

Figure 6(a).

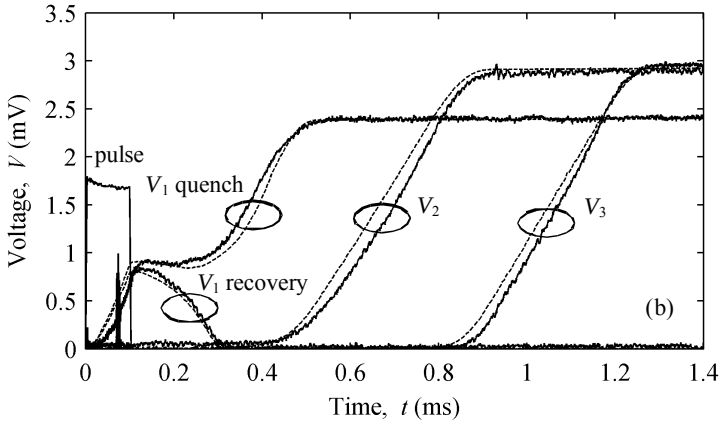

Figure 6(b).

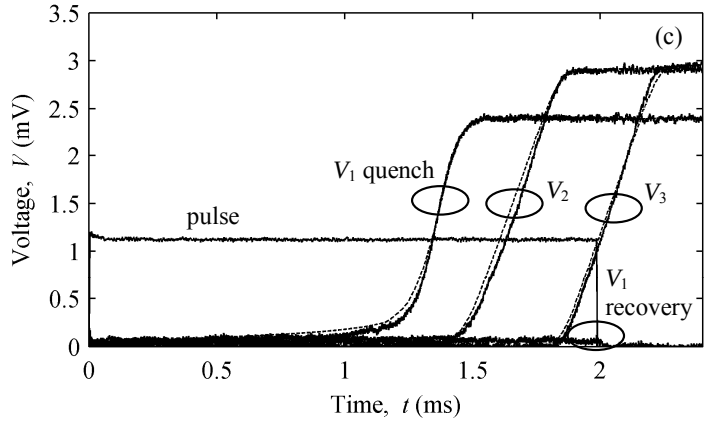

Figure 6(c).

Measured (solid) and computed (dashed) voltages at 6 T, I_{op} = 85% I_C, t_{pulse} = 50 μs (a), 100 μs (b) and 2000 μs (c) for the NbTi wire.

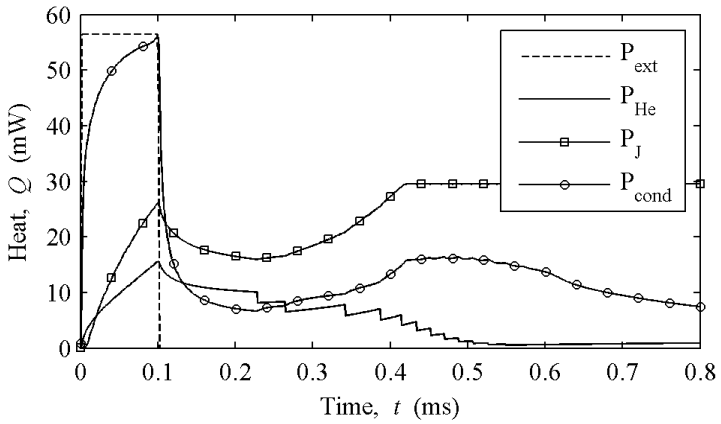

Figure 7. Heat fluxes exchanged with the environment by the central wire sector in the quench case reported in Fig. 6b.

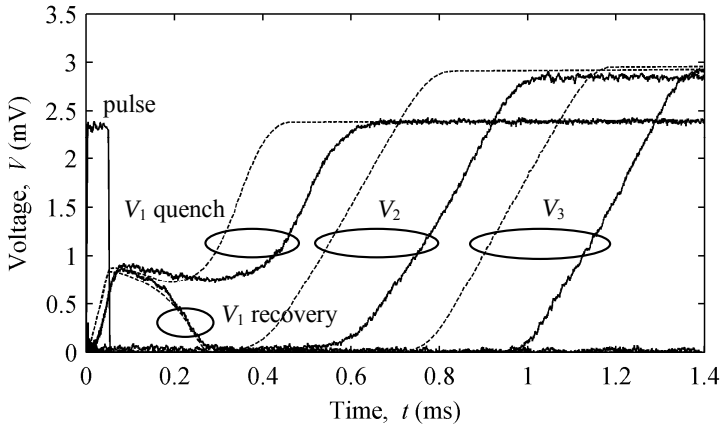

Figure 8. Improvement of the agreement with experimental data obtained changing σ from 0 mm (a) to 1 mm (b).

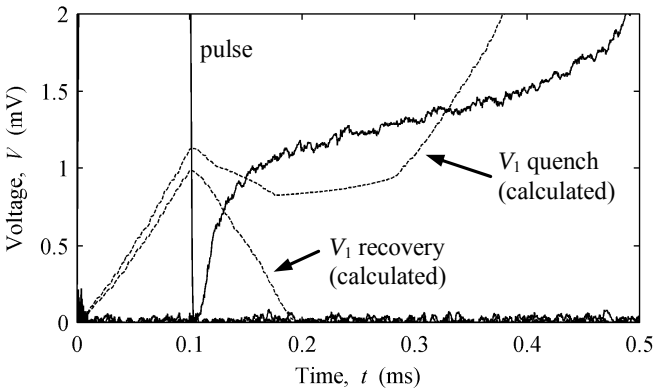

Figure 9. Disagreement between simulation and experiment in the application of the uniform temperature model to the analysis of quench development in the Nb_3Sn wire.

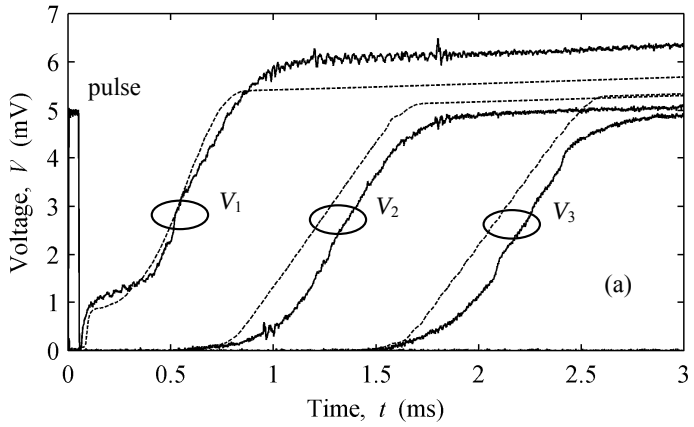

Figure 10(a).

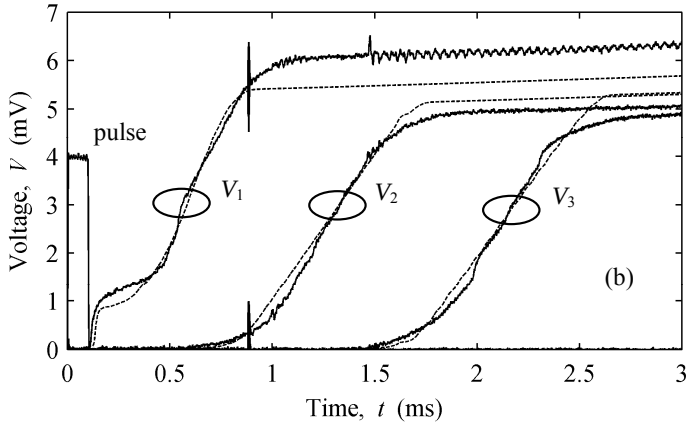

Figure 10(b).

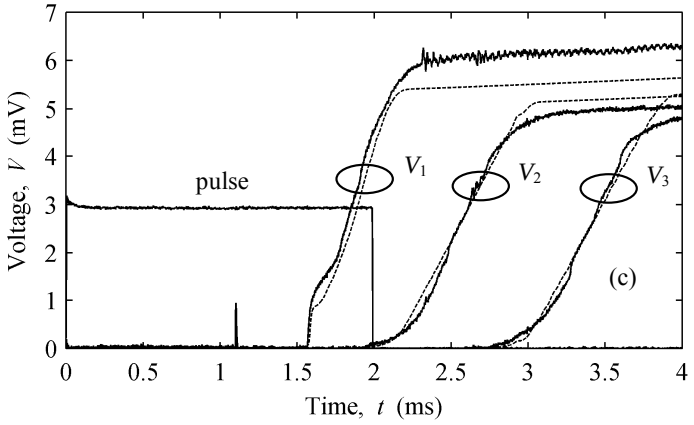

Figure 10(c).

Measured (solid) and computed (dashed) voltages at 7 T, I_{op} = 85% I_C, t_{pulse} = 50 μs (a), 100 μs (b) and 2000 μs (c) for the Nb_3Sn wire.

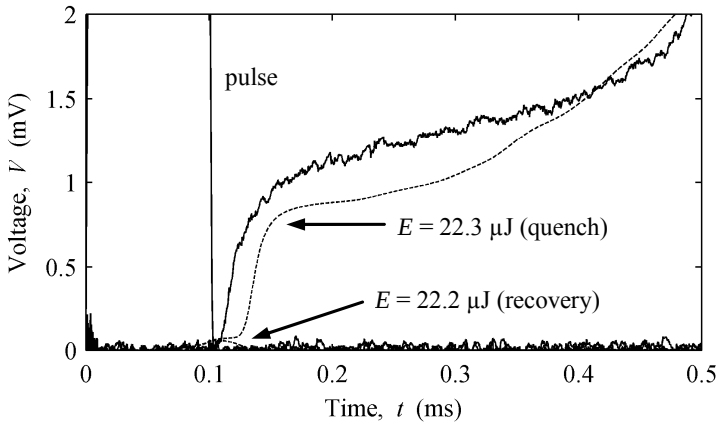

Figure 11. Magnification of Fig. 10(b), showing the abrupt transition between quench and no quench behavior with slight variation of the input energy (0.1 μJ) in Nb_3Sn wire.

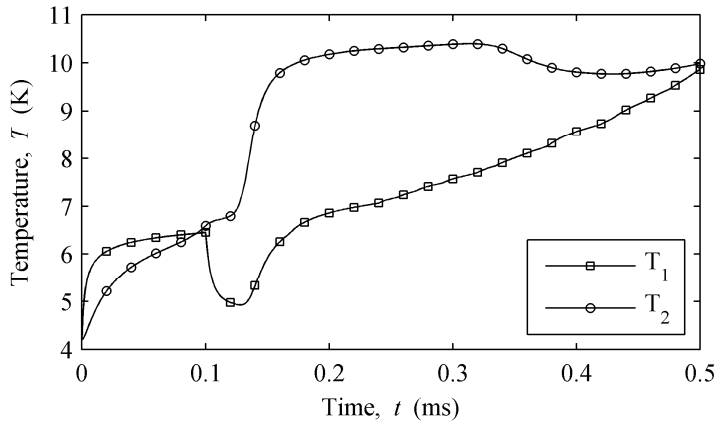

Figure 12. Evolution of T_1 and T_2 of the central illuminated wire sector for the quench simulation reported in Fig. 10(b).

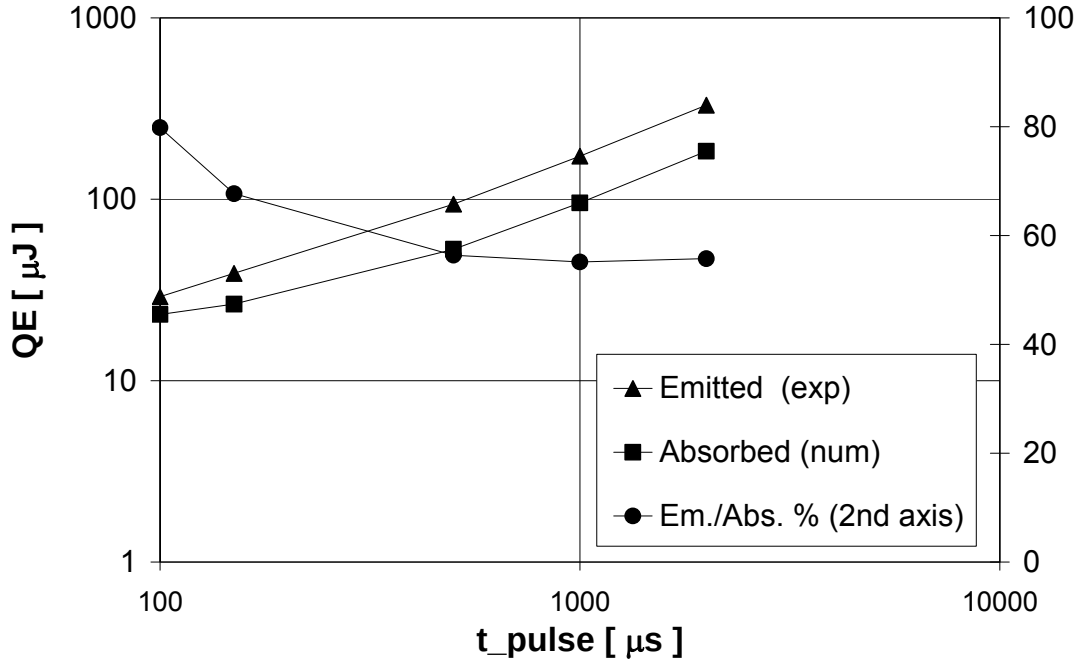

Figure 13. Measured and computed QEs for NbTi wire at 6 T, I_{op} = 85% I_C, and different values of t_{pulse}.

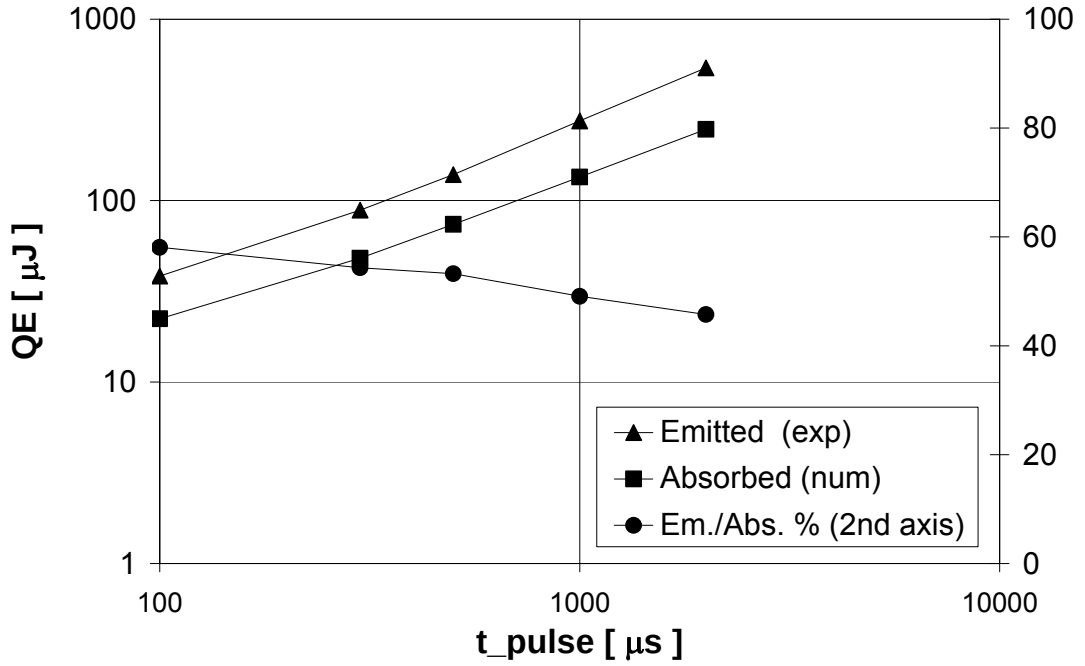

Figure 14. Measured and computed QEs for Nb_3Sn wire at 7 T, I_{op} = 85% I_C, and different values of t_{pulse}.

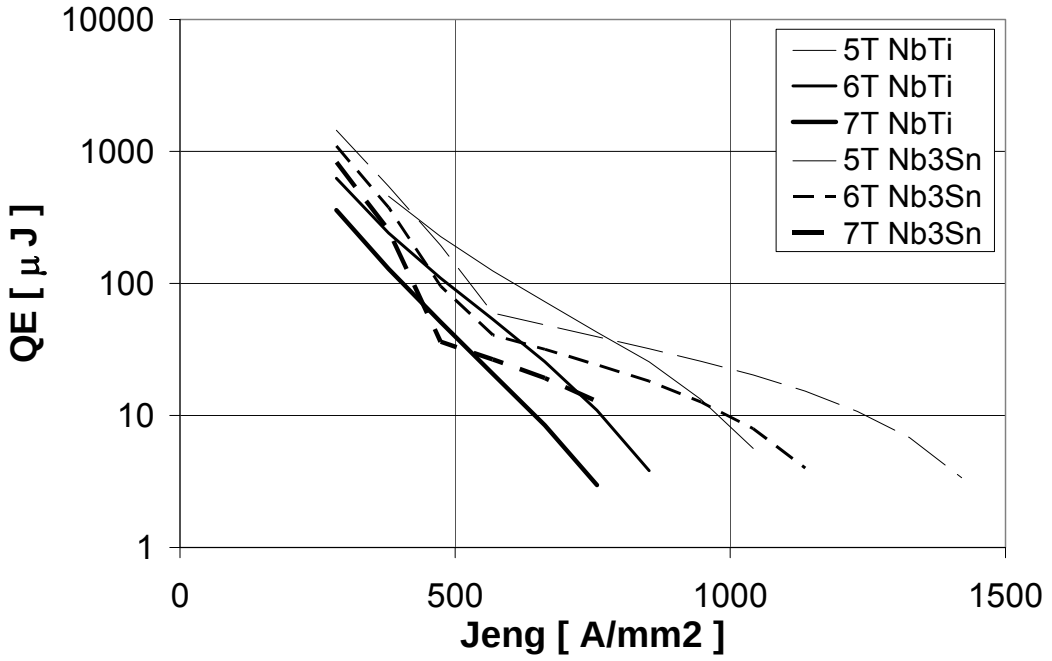

Figure 15. Comparison of the calculated QEs for the NbTi and the Nb_3Sn wire at different background fields and engineering current densities.

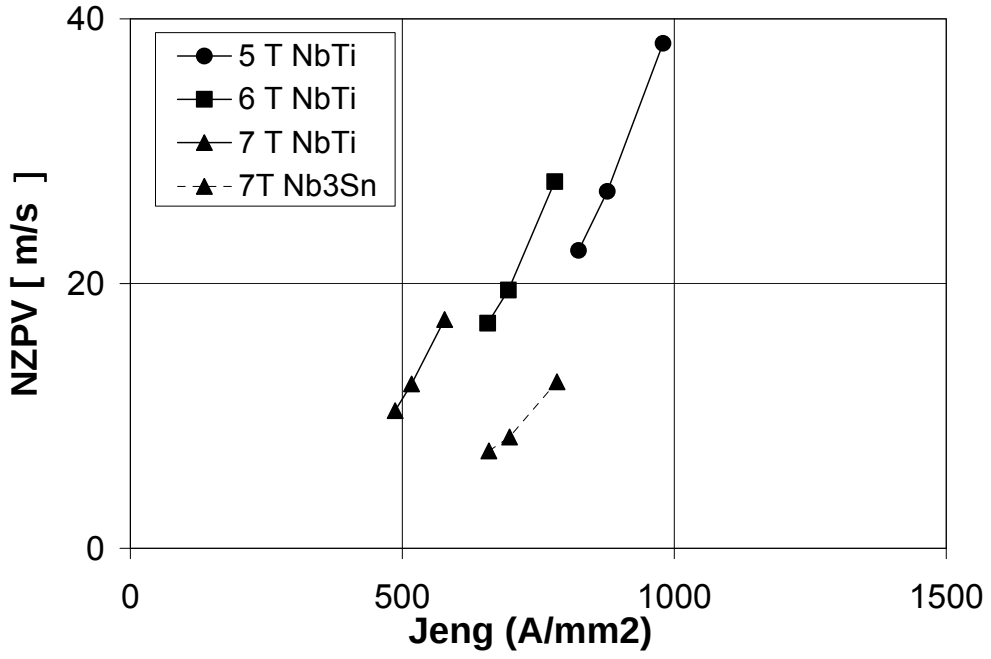

Figure 16. Comparison of the measured NZPVs for the NbTi and the Nb_3Sn wire at different background fields and engineering current densities.